Article

Green Synthesis of Fe_3O_4 Nanoparticles and Its Applications in Wastewater Treatment

Shahnaz Bassim [1], Alyaa K. Mageed [1], Adnan A. AbdulRazak [1,*] and Hasan Sh. Majdi [2]

1 Department of Chemical Engineering, University of Technology, Baghdad 10066, Iraq
2 Chemical Engineering and Oil Refinery Department, Al Mustaqbal University College, Hilla, Babylon 51001, Iraq
* Correspondence: adnan.a.alsalim@uotechnology.edu.iq

Abstract: In this paper, the extract of *Citrus aurantium* (CA) was used as a green approach for the preparation of Fe_3O_4 nanoparticles. The green Fe_3O_4 (Fe_3O_4/CA) was characterized by X-ray diffraction (XRD), scanning electron microscopy (SEM), energy-dispersive X-ray spectroscopy analysis (EDX), Fourier-transform infrared (FTIR) spectroscopy, Brunauer–Emmett–Teller (BET) surface area measurement, and vibrating sample magnetometry (VSM). The synthesized Fe_3O_4/CA was used to remove methylene blue (MB) dye from an aqueous solution. A four-factor central composite design (CCD), combined with response surface modeling (RSM), was used to maximize the MB dye removal. The four independent variables, which were initial dye concentration (10–50 mg/L), solution pH (3–9), adsorbent dose (ranging from 200–1000 mg/L), and contact time (30–90 min), were used as inputs to the model of the perecentage dye removal. The results yielded by an analysis of variance (ANOVA) confirmed the high significance of the regression model. The predicted values of the MB dye removal were in agreement with the corresponding experimental values. Optimized conditions for the maximum MB dye removal (93.14%) by Fe_3O_4/CA were the initial dye concentration (10.02 mg/L), pH (8.98), adsorbent mass (997.99 mg/L), and contact time (43.71 min). The validity of the quadratic model was examined, and good agreement was found between the experimental and predicted values. Our findings demonstrated that green Fe_3O_4NPs is a good adsorbent for MB removal.

Keywords: *Citrus aurantium*; green synthesis; Fe_3O_4 nanoparticles; methylene blue; adsorption

1. Introduction

Growth in the global population and rapid technological development has produced environmental disruption and pollution increased, with contaminated water being the most common sort of environmental pollution [1]. More than 100,000 commercially available dyes are projected to be generated annually, with over 7×10^5 tons of dyestuff produced every year [2]. It is widely acknowledged that dyes and heavy metals have a significant impact on public perceptions of water quality [3,4]. Dyes are pollutants that are produced by the leather, paper, textile, plastic, rubber, and printing industries. Dyes are classed based on a variety of variables, including the molecule charge, nature of cation (e.g., methyl blue or MB), and nature of anion (e.g., Orange G) [5]. MB is the significant material used in dyes for wood, cotton, and silk.

MB can cause eye burns, which can result in irreversible ocular damage, MB's inhalation can induce rapid or difficult breathing for a short time, and swallow over the mouth causes a burning feeling, nausea, vomiting, intense sweating, methemoglobinemia, and mental disorientation. Due to the MB adverse effects on receiving waterways, the wastewater treatment containing MB dye is of great interest and importance [6].

There are many methods for degrading dyes in wastewater, including chemical, physical, and biological approaches, but most of these methods have high degradation and maintenance costs, and some produce secondary waste products that require further

treatment, so they are not suitable or cost-effective for wastewater treatment [7]. Adsorption is a well-known separation process that can be used to decontaminate water [8]. This process has been proven to be superior to other techniques for water reuse due to its low initial cost, simplicity and flexibility of design, sensitivity to harmful pollutants, ease of operation, and because it does not lead to the creation of any hazardous chemicals [9–12].

Recently, several methods have been investigated for the production of less expensive and effective adsorbents. Several researchers have proposed a variety of nontraditional, low-cost adsorbents, including natural materials, biosorbents, and waste materials from agriculture and industry, these materials could be used to remove colors from solutions as adsorbents [13].

Iron oxides are the most common transition metal oxides, and they have several technological applications. The most frequently occurring iron oxides are magnetite (Fe_3O_4), maghemite (γ-Fe_2O_3), and hematite, (α-Fe_2O_3) [14]. Due to the existence of iron cations in two valence states (i.e., Fe^{+3} and Fe^{+2}) in the inverse spinel structure, magnetite Fe_3O_4 has the most potentially useful features of all iron oxides. At temperatures below 858 $^\circ$K, the cubic spinel Fe_3O_4 is ferromagnetic [15]. Magnetite nanoparticles, however, have two key problems: Fast agglomeration and oxidation by atmospheric oxygen.

Coprecipitation has been reported for the synthesis of Fe_3O_4 nanoparticles (NPs) [16]. As reducing agents, chemicals such as hydrazine, dimethyl formamide, sodium borohydride, and carbon monoxide have been used in this synthetic method. These chemicals have both environmental and biological consequences. Therefore, it is particularly desirable to synthesise Fe_3O_4 NPs by utilizing a green strategy from nontoxic, environmentally friendly ingredients [17]. Plant-mediated green nanoparticle synthesis has lately gained a great deal of attention as a cost-effective and environmentally friendly alternative to physical and chemical approaches. There are several studies of plant-mediated Fe_3O_4 NP production that used various plant extracts, such as grape proanthocyanidin seed extract [18], gum Arabic [19], Sapinduss Mukkorossi Fruits [20], Chlorella-K01 extract [21], and leaf extract of Zanthoxylum armatum DC [22]. However, no literature review is available for the synthesis of Fe_3O_4 NPs using citrus aurantium extract. This eco-friendly methodology offers a facile synthesis at low cost and non-toxic alternative to obtaining magnetic materials.

One of the largest species of plants is Citrus; it consists of 40 species, which are distributed in all continents [23]. Citrus fruits are members of the Rutaceae family, and many citrus varieties, including sweet orange, grapefruit, lemon, bitter orange juice (Citrus aurantium), and kiwi, have become increasingly popular for scientific applications in recent years [24]. Bitter orange juice was analyzed by Karadeniz (2004), he found the following composition: Malic acid 2.21 g/L, citric acid 48.79 g/L, titratable acidity 48.48 g/L, pH 2.60, and total soluble solids (Brix) 10 [25].

In this paper, we present a straightforward and environmentally friendly approach for synthesizing Fe_3O_4 NPs using *Citrus aurantium* juice extract, where the green Fe_3O_4 NPs were used to remove MB dye from an aqueous solution.

2. Materials and Methods

2.1. Materials

2.1.1. Chemicals

Citrus aurantium juice extract was obtained from Baghdad, Iraq. The materials used in the experiments included ferrous sulfate heptahydrate ($FeSO_4.7H_2O$), ferric chloride ($FeCl_3.6H_2O$), ammonium hydroxide (NH_4OH), sodium hydroxide (NaOH), sodium chloride (NaCl), hydrochloride acid (HCl), and methylene blue ($C_{16}H_{18}CIN_3S.XH_2O$). In this study, all chemicals and reagents used were of analytical reagent grade, which were purchased from HiMedia (Thane, India).

2.1.2. Preparation of *Citrus aurantium* (CA) Juice

To manufacture the extract *Citrus aurantium*, 5 kg of *Citrus aurantium* was thoroughly washed with distilled water to remove any dust, after which it was cut and squeezed to

extract the juice. Then, it was heated for 30 min at 80 °C. After being cooled to room temperature, filter paper was used to remove the remaining sediment. Later, it was stored as pure extract without the filler for more experimental work.

2.1.3. Preparation of Fe_3O_4

In this study, Fe_3O_4 NPs were synthesized using a conventional coprecipitation method [26] and a green method that used with *Citrus aurantium* juice extract, denoted as Fe_3O_4 NPs and Fe_3O_4/CA, respectively. In the synthesized Fe_3O_4/CA, 10 mL of 0.25 M $FeSO_4.7H_2O$ was mixed with 20 mL of 0.25 M $FeCl_3.6H_2O$, and 50 mL of juice extract was added under continuous mixing for 30 min. Then, 30 mL (12 M) of ammonia (NH_4OH) was added to the mixture, and mixing continued for 1 h at 80 °C until the color of the solution changed to a dark brown.

2.1.4. Characterization

To characterize the Fe_3O_4 NPs and Fe_3O_4/CA samples, Energy-dispersive X-ray spectroscopy analysis (EDX), scanning electron microscopy (SEM), X-ray diffraction (XRD), vibrating sample magnetometry (VSM), and Brunauer–Emmett–Teller (BET) measurements were done. EDX and SEM analyses were conducted using a Bruker INSPECT550 (Leiderdorp, The Netherlands). The XRD measurements were conducted by Shimadzu-6000 (Kyoto, Japan) at the Cu Kα wavelength (λ = 0.1524 nm) with 2θ scaled from 5 to 80°. The sample magnetic measurement was performed using a magnetometer (VSM1100, Weistron, Hsinchu City, Taiwan), and the hysteresis loops were obtained at 298 °K by applying a maximum magnetic field of 60 kOe. In addition, the Brunauer–Emmett–Teller (BET) method was conducted using the (type: Q-surf 9600, origin: USA).

2.2. Experimental Design

In this study, Design-Expert 7.0.0 software (Stat-Ease Inc., Minneapolis, MN, USA) was used, where the central composite design (CCD) using a response surface methodology (RSM) was applied to correlate and optimize the four operation process variables (i.e., initial dye concentration; solution pH; adsorbent dose; and contact time) in relation to the dye removal. The minimum and maximum ranges of the four operational process variables were the initial dye concentration (A) (10–50 mg/L), solution pH (B) (3–9), adsorbent dose (C) (200–1000 mg/L), and contact time (D) (30–90 min). Table 1 presents the high, center, and low levels of the four independent variables investigated in this study. The details of the data for each of the 30 runs are presented in Table 2.

Table 1. High, center and low levels of the independent variables investigated in the present study.

Variables	Levels and Range		
	(+1)	**(0)**	**(+1)**
Initial dye concontration (A) (mg/L)	10	30	50
Solution pH (B)	3	6	9
Adsorbent dose (C) (mg/L)	200	600	1000
Contact time (D) (min)	30	60	90

Table 2. Experimental design data in relation to perecentage dye removal.

Run No.	A: Initial Con. (mg/L)	B: pH	C: Adsorbent Dose (mg/L)	D: Time (min)	Dye Removal (%)
1	30.00	6.00	600.00	90.00	66.1
2	30.00	9.00	600.00	60.00	80.2
3	30.00	6.00	600.00	60.00	61.99
4	50.00	3.00	1000.00	30.00	55.5
5	10.00	3.00	200.00	90.00	35.6
6	50.00	3.00	1000.00	90.00	75
7	30.00	6.00	200.00	60.00	48.45
8	30.00	6.00	600.00	60.00	61.99
9	50.00	9.00	1000.00	90.00	87.6
10	30.00	6.00	600.00	30.00	53.66
11	10.00	9.00	200.00	30.00	89.4
12	30.00	6.00	600.00	60.00	61.99
13	10.00	9.00	1000.00	30.00	89.73
14	50.00	6.00	600.00	60.00	56.34
15	30.00	6.00	600.00	60.00	61.99
16	30.00	6.00	600.00	60.00	61.99
17	50.00	9.00	200.00	30.00	62.6
18	10.00	3.00	1000.00	90.00	68.7
19	30.00	6.00	600.00	60.00	61.99
20	30.00	3.00	600.00	60.00	45.36
21	50.00	9.00	1000.00	30.00	65.78
22	10.00	3.00	1000.00	30.00	56.21
23	10.00	9.00	1000.00	90.00	93
24	10.00	6.00	600.00	60.00	68.8
25	30.00	6.00	1000.00	60.00	78
26	10.00	3.00	200.00	30.00	20.4
27	50.00	3.00	200.00	90.00	40.74
28	50.00	9.00	200.00	90.00	69.54
29	50.00	3.00	200.00	30.00	23.99
30	10.00	9.00	200.00	90.00	91.3

2.3. Batch Adsorption Studies

The removal of MB was randomly conducted by employing batch experiments in an aqueous solution using an adsorbent, which is Fe_3O_4/CA. Experiments of adsorption were carried out in a shaker (KS10, Edmund Buhler, Bodelshausen, Germany) at 300 rpm, where 200-mL conical flasks were filled with 50 mL of the MB solution of a known initial concentration (10–50 mg/L), and a specific mass of Fe_3O_4 (200–1000 mg/L) was added at a controlled pH level (3–9) for a contact time of 30–120 min. The supernatant was separated by centrifuge when the equilibrium was attained.

The pH of the solution was measured using a pH 9124 electronic device made by HANNA (Woonsocket, RI, USA) and adjusted by adding 0.1 M hydrochloric acid or 0.1 M sodium hydroxide to the dye solution. The experiment was balanced by taking a sample at regular time intervals. The solution was filtered using a centrifuge at 10,000 rpm for

15 min. A UV-visible spectrophotometer (λmax-664 nm) was used to calculate the dye concentration and the ratio of the perecentage removal by Equation (1):

$$\% \text{ dye removal} = \frac{Ci - Co}{Ci} \times 100 \tag{1}$$

where *Ci* and *Co* are the initial and final concentration of MB, respectively.

3. Results and Discussion

3.1. Characterization of Fe$_3$O$_4$ NPs/CA

The FTIR spectra of Fe$_3$O$_4$/CA, and Fe$_3$O$_4$/CA after the adsorption of MB are presented in Figure 1a,b. The FTIR spectra of Fe$_3$O$_4$/CA exhibited intense peaks between 580 cm^{-1} and 630 cm^{-1}, which are attributed to the stretching vibration mode associated with the bonds of Fe–O in the Fe$_3$O$_4$ crystal lattice [27]. At 1629 cm^{-1} and 3435 cm^{-1}, there are band and broad band due to the hydroxyl groups, OH–bending and OH–stretching, respectively [28]. Other bands were observed in the spectra of Fe$_3$O$_4$/CA. The peak in Figure 1a at 1562.34 cm^{-1} refers to the C=C stretching vibration in the aromatic C–C bond. The peak at 1562.34 cm^{-1} indicates that impregnation with Fe$_3$O$_4$ NPs led to an increase in the aromatic properties. The peaks at 1415.75 cm^{-1} and 1327.03 cm^{-1} are attributed to the bending and stretching vibrations of CH$_2$ and C–N bonds of the Fe$_3$O$_4$ NPs [29,30], while the peak between 1157.29 cm^{-1} and 1114.86 cm^{-1} is attributed to the stretching between C–O and O–H for –COOH [31]. After adsorption of MB over Fe$_3$O$_4$/CA, the FTIR spectrum showed a minor shift of band locations and decreased in intensity in comparison to fresh Fe$_3$O$_4$/CA, clearly confirming the MB adsorption over Fe$_3$O$_4$/CA and the adsorptive binding of MB with Fe$_3$O$_4$/CA, which may be governed by electrostatic interaction electron rich oxygen of Fe$_3$O$_4$/CA and MB cations, as demonstrated in Figure 1b. In addition, effective functional groups appeared at 1041.56 cm^{-1} as a sulfoxide (S=O), which confirm the presence of MB dye on Fe$_3$O$_4$/CA.

The vibrating sample magnetometry (VSM) hysteresis loop magnetization curve was produced using a magnetometer at 298 °K. Figure 2 shows the magnetization curve of Fe$_3$O$_4$/CA, which confirms the superparamagnetic behavior. The resulting saturation magnetization value of 24.5 emu/g is in agreement with the magnetic nanoparticle's known values [32].

The pattern of XRD for the Fe$_3$O$_4$/CA is presented in Figure 3. The magnetite characteristic peak can be seen at 2θ = 30.3°, 35.8°, 43.01°, 54.14°, 57.5°, and 62.6°, the 2θ of 35.8° is the high intensity. These diffraction peaks are according to the corresponding indices of (220), (311), (400), (422), (511), and (440), and a comparison with the JCPDS card No. 79-0418 indicates that Fe$_3$O$_4$/CA particles clearly matched to Fe$_3$O$_4$. An equation of Scherrer was applied for calculating the average of the crystal size, as follows [33]:

$$D_c = \frac{K\,\lambda}{\beta/2cos\theta} \tag{2}$$

where D_c is the crystalline diameter in nm; *K* is the Scherrer constant; λ is the wavelength of the X-ray radiation; β is the FWHM of the diffraction peak; and θ is the peak diffraction angle. The average crystallite size was computed to be 12.5 nm.
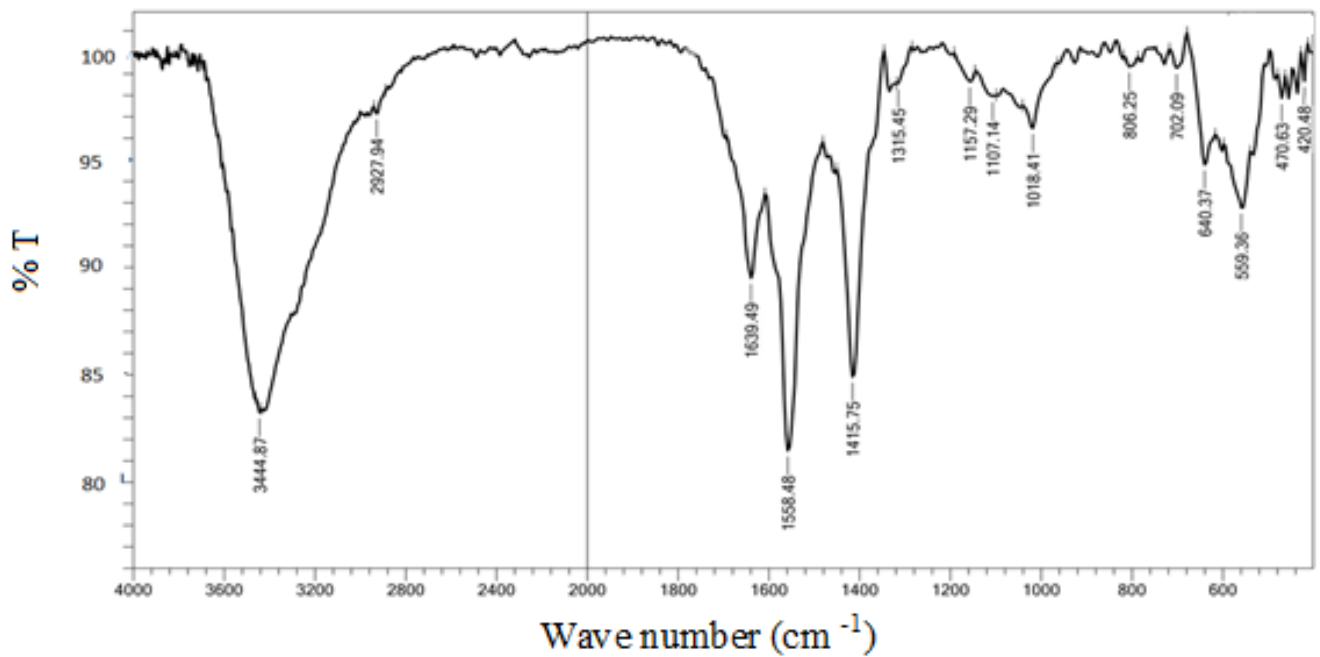
(**a**)
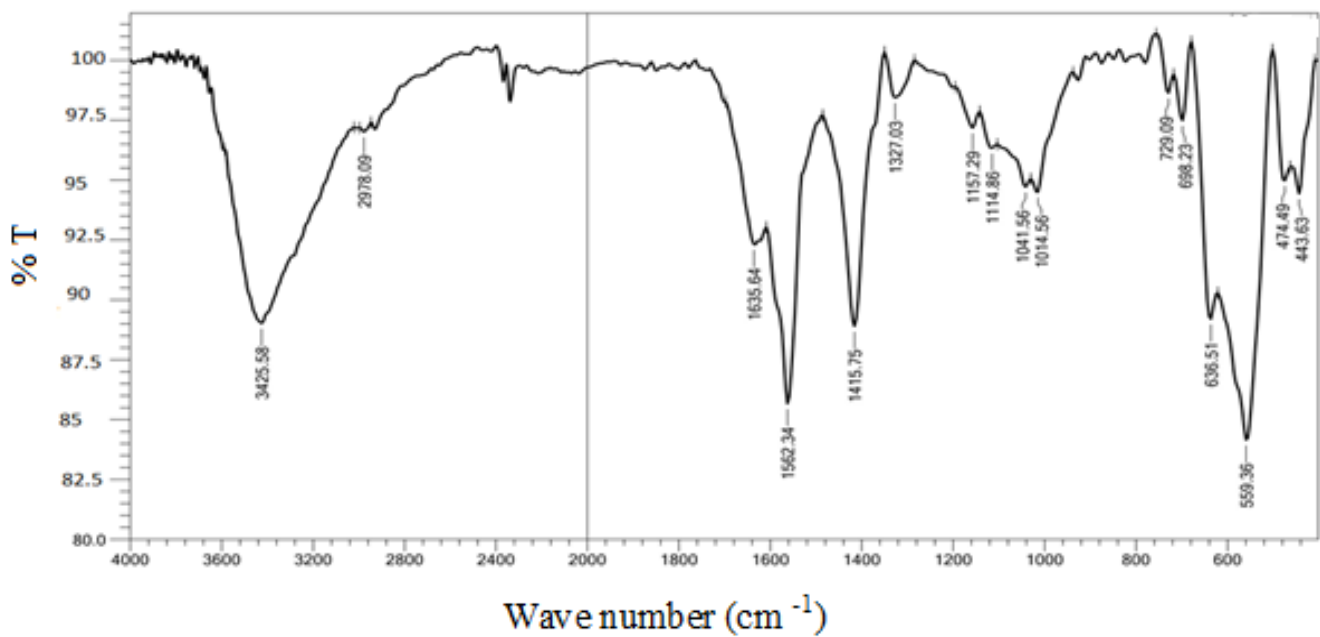
(**b**)

Figure 1. FTIR spectra of (**a**) Fe_3O_4/CA and (**b**) Fe_3O_4/CA after adsorption.
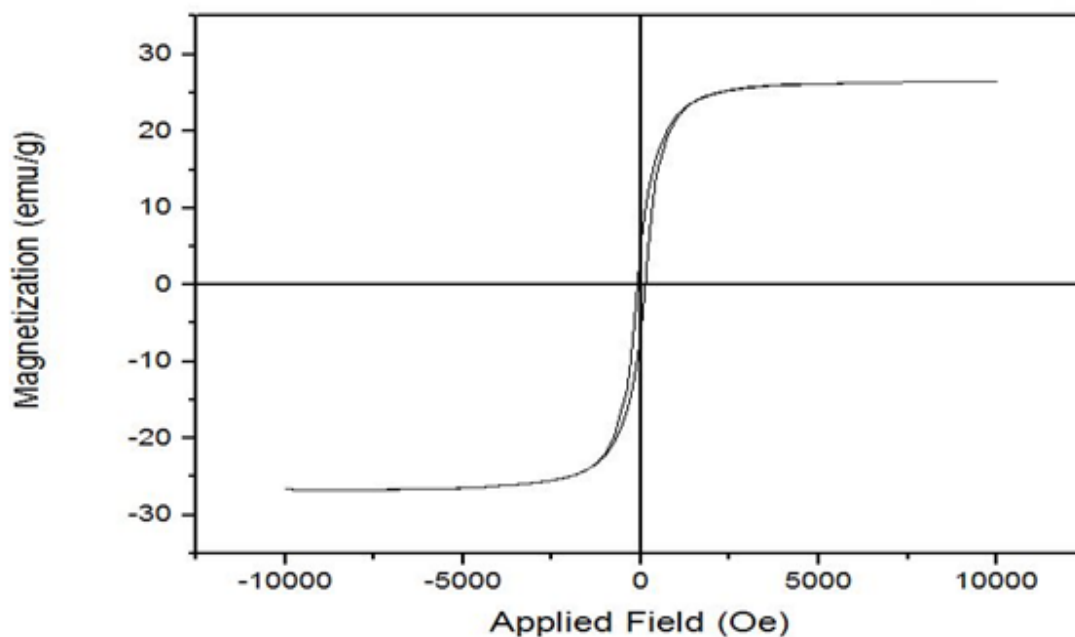
Figure 2. Fe_3O_4/CA hysteresis.
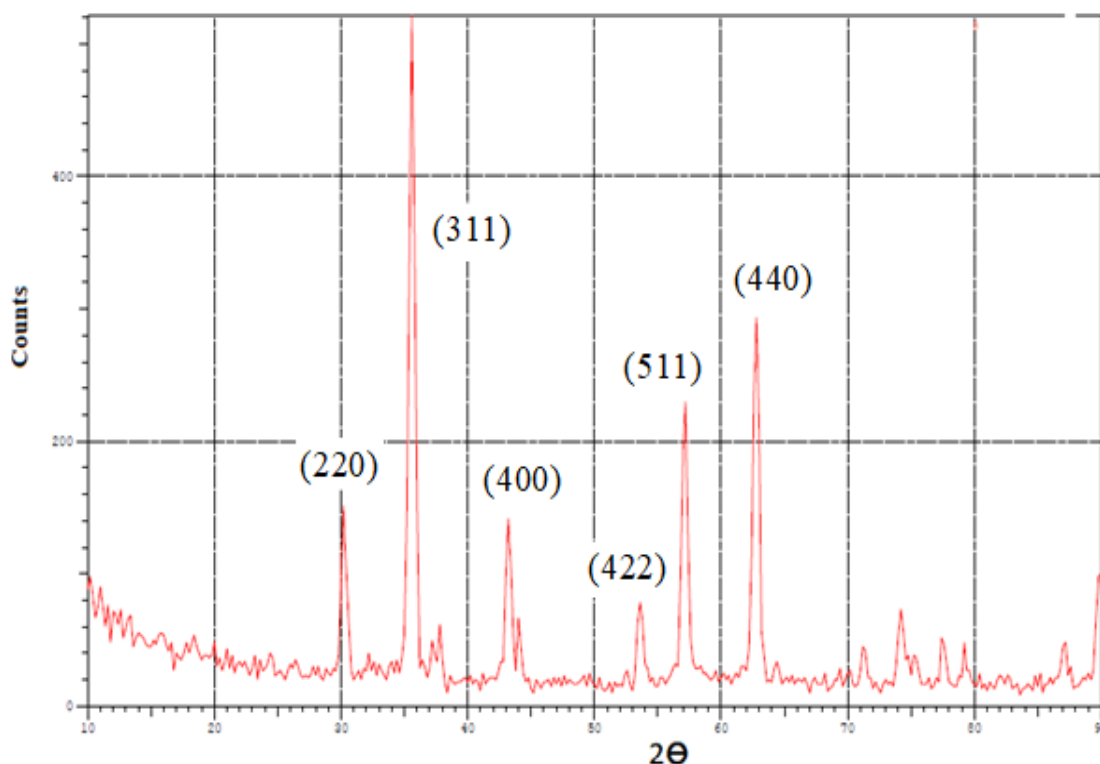
Figure 3. XRD of Fe_3O_4/CA.

Figure 4 shows the surface morphology of the Fe_3O_4 NPs and Fe_3O_4/CA. These indicate that the Fe_3O_4 NPs were predominantly spherical nanoparticles of approximately similar diameters (Figure 4a). In contrast, Figure 4b shows that Fe_3O_4/CA particles were exposed to some aggregation. In most cases, this agglomeration is caused by the lack of a capping agent in the plant extract used in the nanoparticle manufacturing [34]; however, these agglomerations are commonly recognized as overlapping pieces held together by weak Van der Waals forces [35].
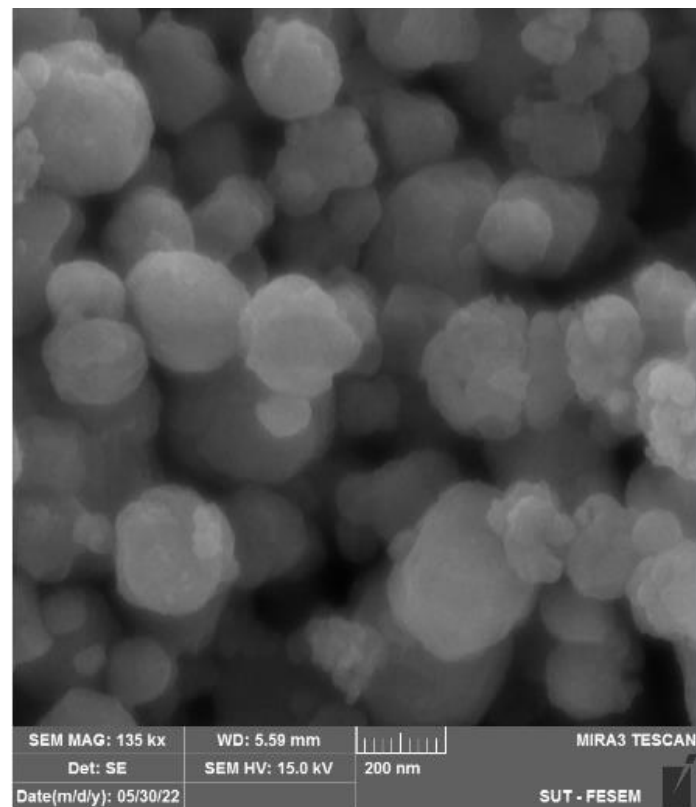
(**a**)
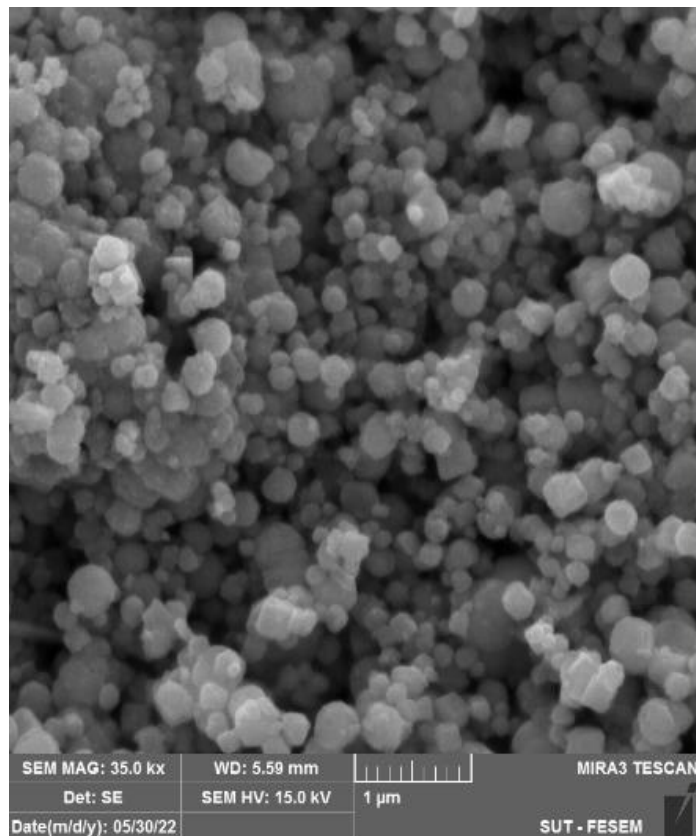
(**b**)

Figure 4. SEM images of (**a**) Fe_3O_4 NPs and (**b**) Fe_3O_4/CA.

From the literature concerning manufacturing Fe_3O_4 using *Rhus coriaria* extract under comparable circumstances, Chen et al. (2013) reported that the majority of Fe_3O_4 particles were large (5–50 m) and asymmetrical [36].

The EDX technique was used to analyze the chemical compositions of the samples. Figure 5 shows the EDX spectrum of Fe_3O_4 NPs after juice loading, which confirms the presence of iron elements in the compounds. The iron percent (72.1) and oxygen percent (19.9) were recorded in the total weight of the Fe_3O_4 NPs, while additional elements occurred in minor amounts.

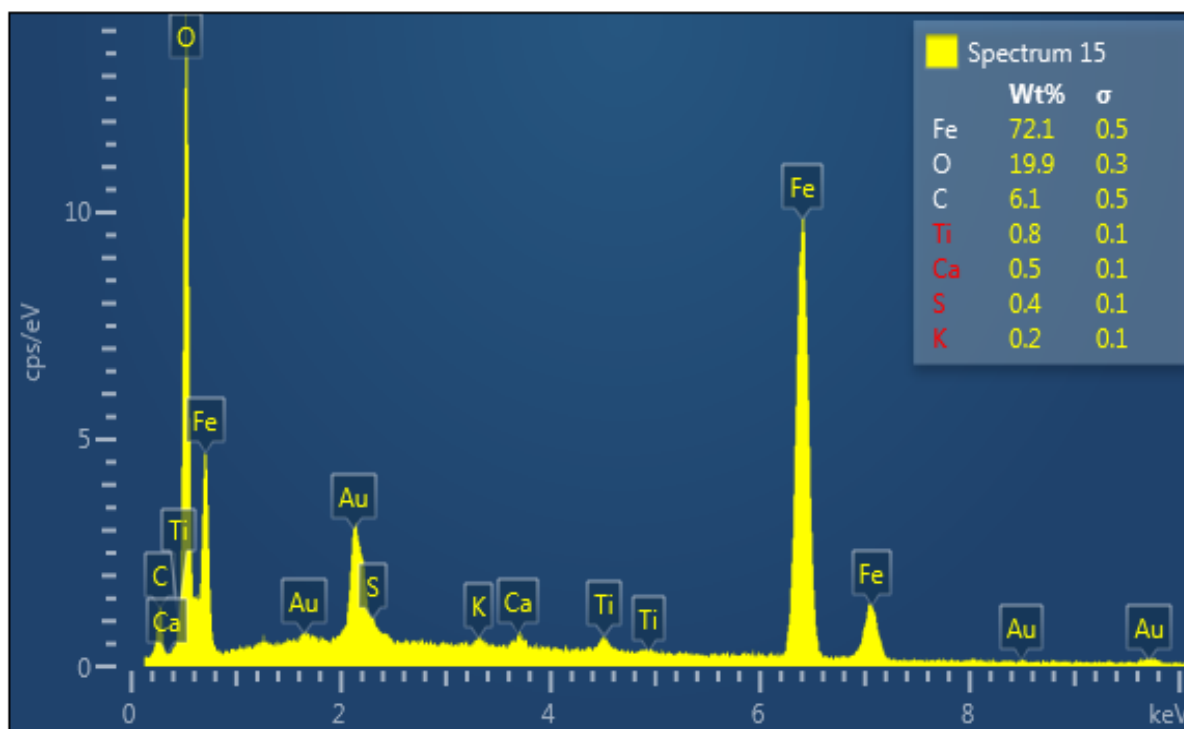**Figure 5.** EDX of the Fe_3O_4 NPs/CA.

Surface features (i.e., specific surface area and pore volume) are crucial elements that must be studied because they have a significant impact on the adsorption capacity. Table 3 provides the BET surface area and pore volume of the Fe_3O_4 and Fe_3O_4/CA. The tabulated results show that the pore volume and surface area of Fe_3O_4/CA were greater than those of Fe_3O_4. The increase in the surface area and pore volume can enhance the adsorbent dye removal efficiency [37].

Table 3. Fe_3O_4 and Fe_3O_4/CA textural properties.

	Fe_3O_4	Fe_3O_4/CA
Surface area (m^2/g)	6.67	32.656
Pore volume (cm^3/g)	0.00472	0.02658

3.2. Regression Model Equation

The experimental results of the perecentage dye removal were modeled using RSM combined with a method of backward, which was performed in Design-Expert 7.0.0 automatically. The developed model for the perecentage dye removal used a second-order polynomial quadratic equation in terms of the coded factors, as follows:

$$\% \text{ dye removal} = +59.63 - 4.22 \times A + 18.66 \times B + 11.60 \times C + 6.13 \times D - 5.76 \times A \times B + 2.01 \times A \times D - 8.53 \times B \times C - 1.88 \times B \times D + 3.16 \times C^2 \quad (3)$$

where A is the initial dye concentration (mg/L), B pertains to the solution pH, C is the dose of adsorbent (mg/L), and D denotes the contact time (min). The above model presents the positive signs point to these variables exerting a positive effect on the perecentage dye removal, whereas negative signs point to the effect of antagonistic on the perecentage dye removal. The positive value relating to the adsorbent dose (B), contact time (C), and solution pH had a positive effect, as these terms increased the perecentage dye removal. Conversely, the negative value relating to the initial dye concentration (A) indicates that it exerted the effect of antagonistic on the perecentage dye removal of Fe_3O_4/CA.

To study the adequacy and significance of the current model, an ANOVA test was performed, with the results presented in Table 4. The *p* value was set at <0.05, and the F-value was high, at 116.16. These results indicate that the second-order quadratic model was adequate for describing the MB removal process using Fe_3O_4/CA. Values of "Prob > F" less than 0.0500 indicate that the model terms are significant. In this case A, B, C, D, AB, AD, BC, BD, CD, and C^2 are significant model terms. An accuracy of the above model was estimated in terms of the regression coefficients (R^2), adjusted R^2, and predicted R^2, which were 0.9812, 0.9728, and 0.9346, respectively.

Table 4. ANOVA results for the MB dye removal model.

Source	Sum of Squares	df	Mean Square	F-Value	*p*-Value Prob > F	
Model	9668.99	9	1074.33	116.16	<0.0001	Significant
A: Initial con. (mg/L)	321.31	1	321.31	34.74	<0.0001	
B: pH	5928.76	1	5928.76	641.01	<0.0001	
C: Adsorbent dose (mg/L)	1071.29	1	1071.29	115.83	<0.0001	
D: Time (min)	676.02	1	676.02	73.09	<0.0001	
AB	531.65	1	531.65	57.48	<0.0001	
AD	64.60	1	64.60	6.98	0.0156	
BC	775.76	1	775.76	83.87	<0.0001	
BD	56.29	1	56.29	6.09	0.0228	
C^2	31.99	1	31.99	3.46	0.0777	
Residual	184.98	20	9.25			
Lack of Fit	184.98	15	12.33			
Pure Error	0.000	5	0.000			
Cor. Total	9853.97	29				
Std. Dev.	3.04		R-Squared		0.9812	
Mean	63.13		Adj. R-Squared		0.9728	
C.V.%	4.82		Pred. R-Squared		0.9346	
PRESS	644.30		Adeq. Precision		43.126	

Actual and predicted values of the perecentage dye removal are shown in Figure 6, supporting an agreement between the observed and predicted values, with similar findings in [8].
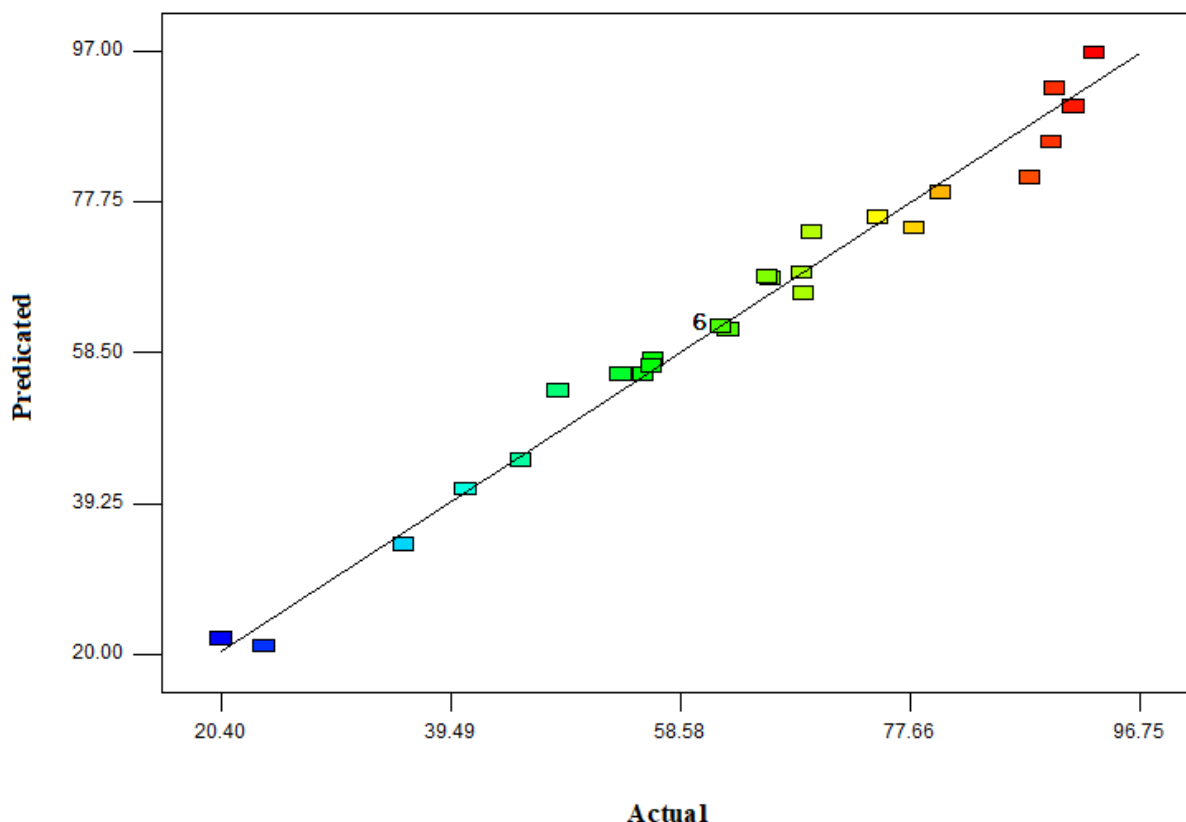
Figure 6. Actual and predicted perecentage of MB removal by Fe_3O_4/CA.

The percentage contributions (PCs) of each independent variable for the perecentage dye removal were estimated using Equation (4) [38] by using the ANOVA results, with the results presented in Table 5. The solution pH (B) showed the highest influence on the perecentage dye removal as its contribution was 62.7%, followed by the adsorbent dose (C) at 11.3%, interaction (BC) at 8.2%, contact time (D) at 7.1%, interaction (AB) at 5.6%, and initial dye concontration (A) at 3.4%. The interaction terms (AD), (BD), and (C^2) had the lowest effects on the perecentage dye removal.
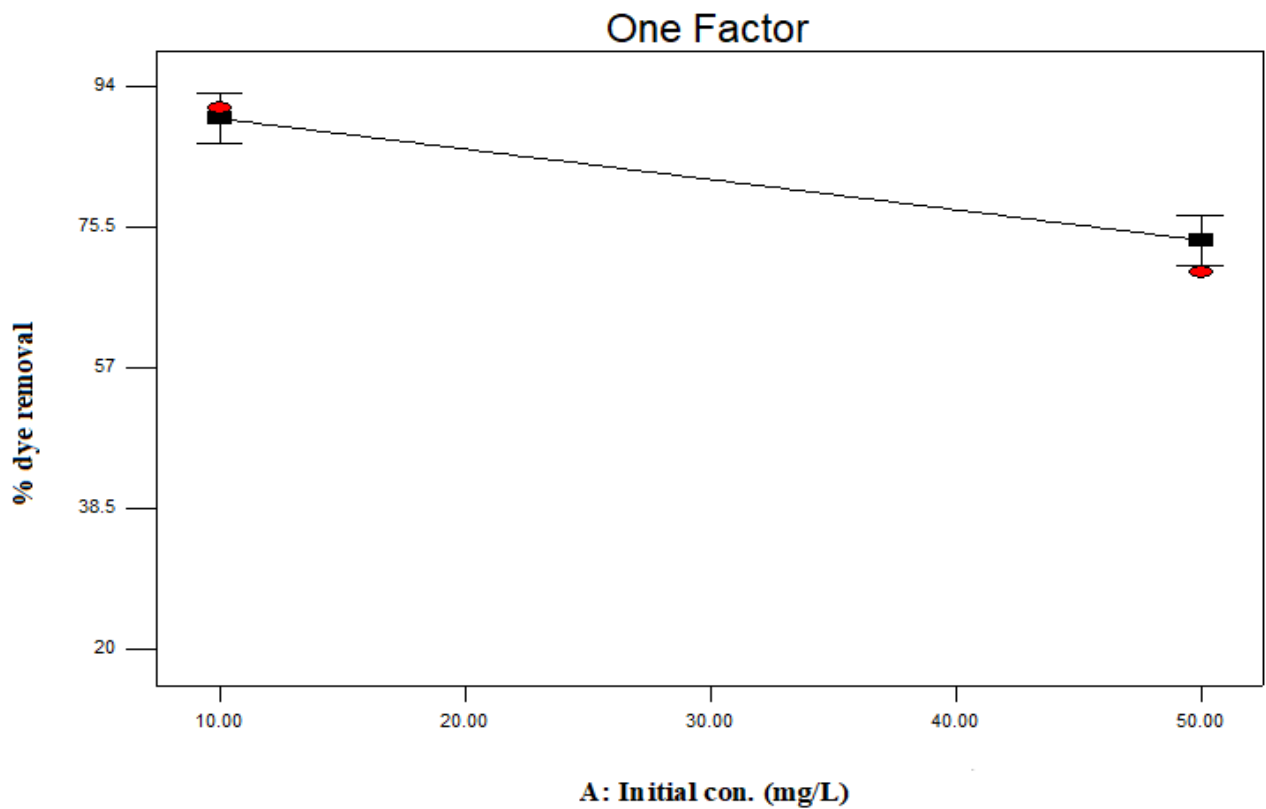
$$PC\% = \frac{SS}{\sum SS} \times 100 \tag{4}$$

where *SS* is the summation of the squares of these terms.

**Table 5.** PC% for current model terms.

| Terms	A	B	C	D	AB	AD	BC	BD	C^2
PC%	3.4	62.7	11.3	7.1	5.6	0.7	8.2	0.6	0.3

3.3. One Factor Plot

Design-Expert 7.0.0 software was used to evaluate the influence of each operation variable on the MB dye removal, as shown in Figures 7–10.
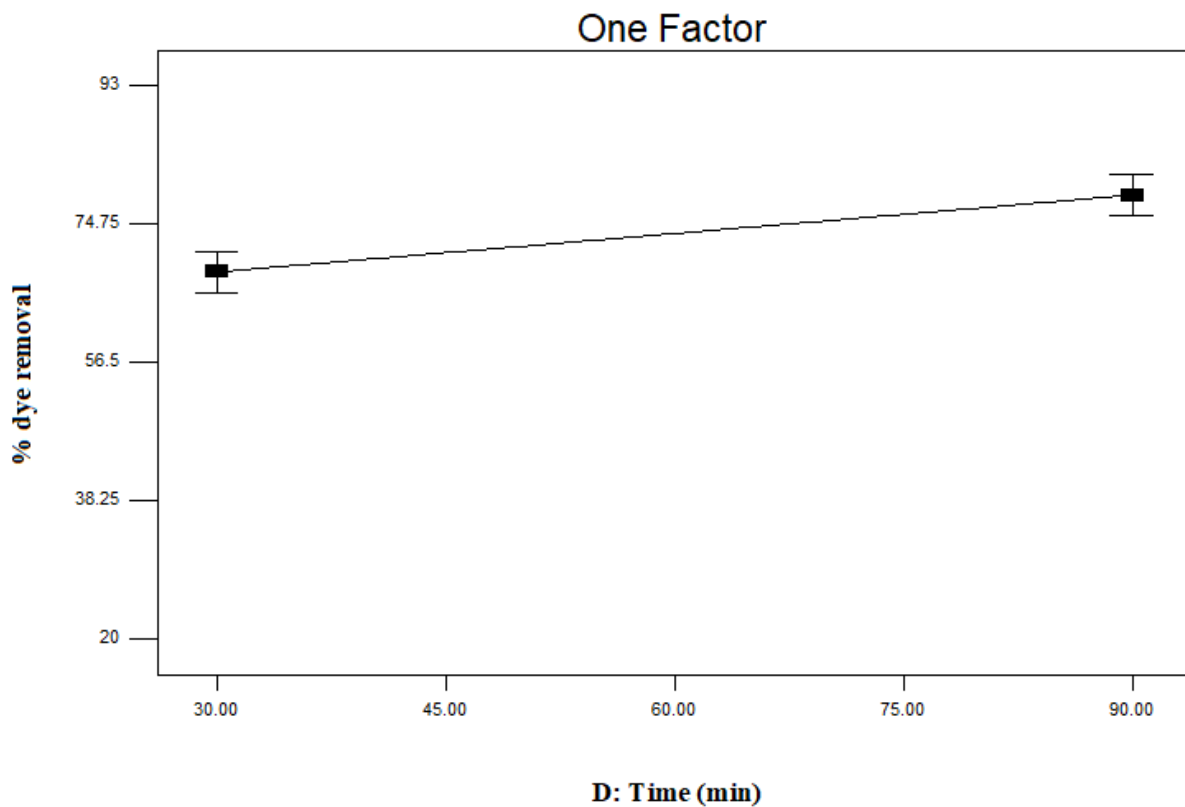
Figure 7. Influence of the initial concontration on the perecentage MB removal at a constant pH (B) of 9, adsorbent dose (C) of 200 mg/L, and time (D) of 89.75 min.
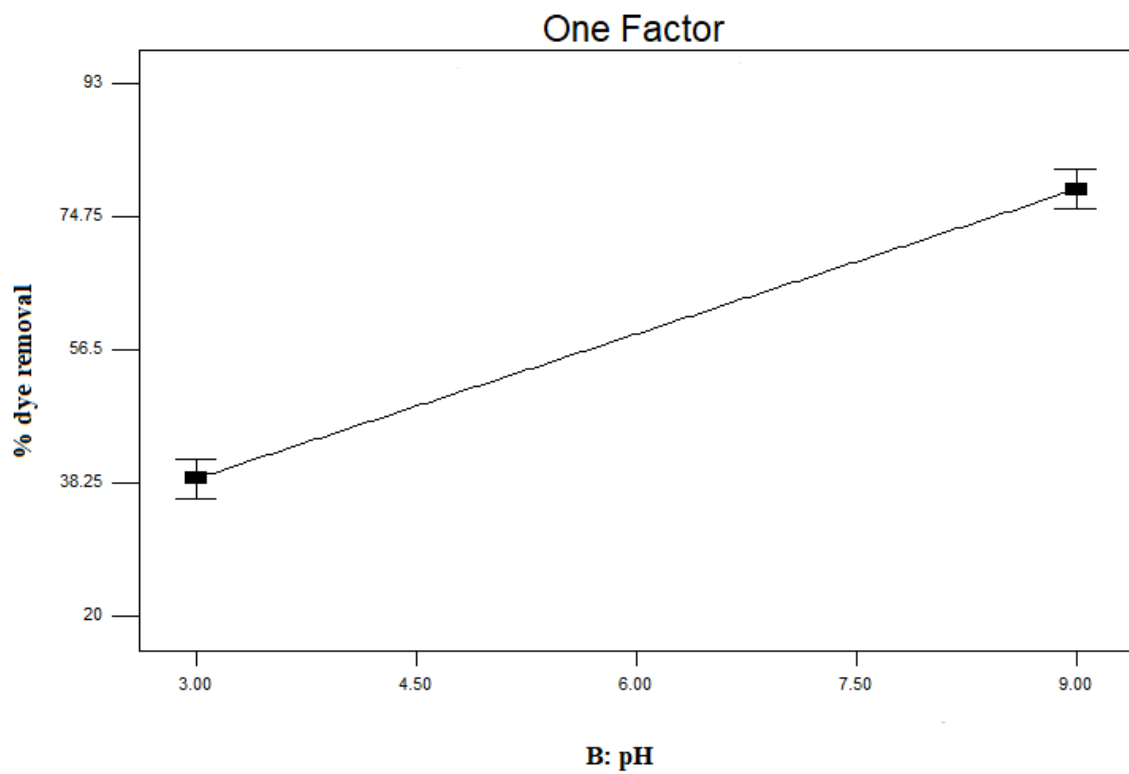
Figure 8. Effect of the solution's pH on the perecentage dye removal at a constant initial dye concentration (A) of 38.19 mg/L, adsorbent dose (C) of 200 mg/L, and time (D) of 89.75 min.
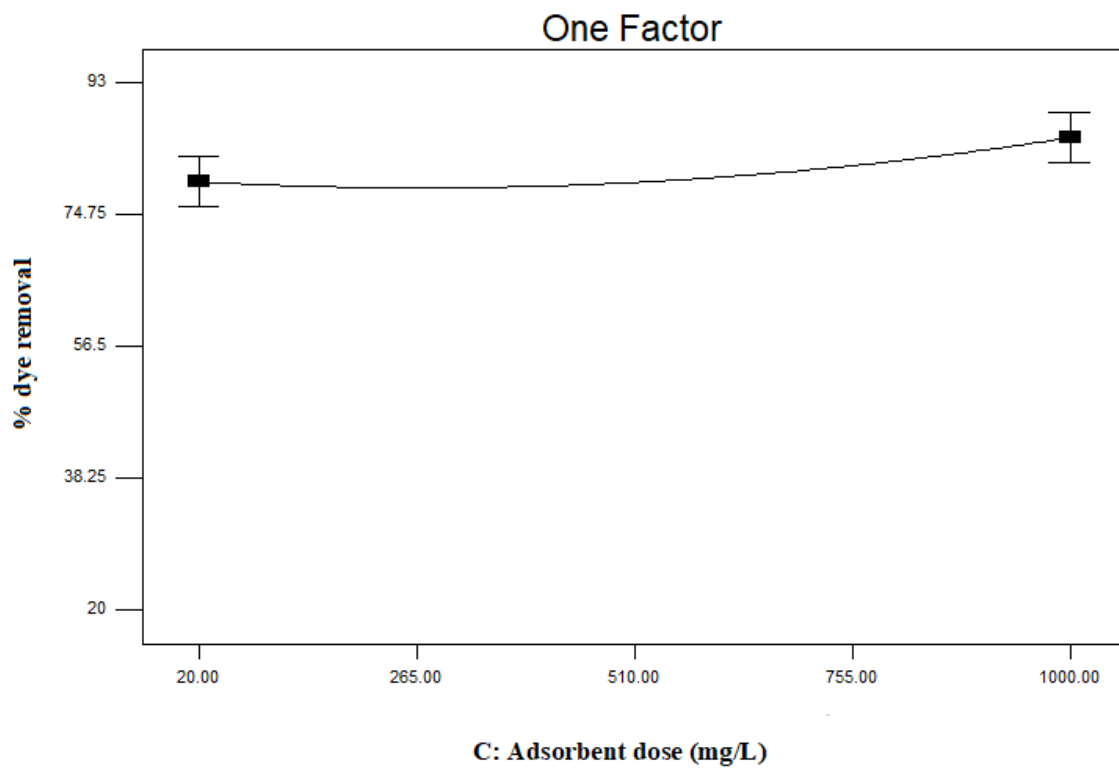
Figure 9. Influence of the adsorbent dose on the perecentage dye removal at a constant initial dye concentration (A) of 38.19 mg/L, pH (B) of nine, and time (D) of 89.75 min.

Figure 10. Effect of time on the perecentage dye removal at a constant initial dye concentration (A) of 38.19 mg/L, pH (B) of nine, and adsorbent dose (C) of 200 mg/L.

Figure 7 shows the influence of the initial dye concontration on the perecentage dye removal at a constant pH (B) of 9, adsorbent dose (C) of 200 mg/L, and time (D) of 89.75 min. The perecentage dye removal decreased from 89.8% to 73.8% as the initial dye concontration increased from 10 to 50 mg/L. Due to a lower initial dye concentration, a higher surface area was obtained due to the smaller number of MB molecules. While with higher dye concentrations, a large number of dye molecules reacted with the accessible adsorption sites. This is in a good agreement with the literature concerning MB removal [12].

Figure 8 shows the effect of the solution pH on the perecentage dye removal, with a constant initial dye concentration (A) of 38.19 mg/L, adsorbent dose (C) of 200 mg/L, and time (D) of 89.75 min. The perecentage dye removal increased from 38.9% to 78.55% as the solution pH increased from three to nine. This occurred because of the influence of the solution's pH on the Fe_3O_4/CA surfaces. At a pH of 9, the negatively charged surface of the Fe_3O_4/CA adsorbed the most cationic dye (MB) because of an increase in the electrostatic attraction between the negative surface charge and the MB dye [12], while, at a pH of three, the protons vied with the MB dyes to adsorb onto the Fe_3O_4/CA surfaces; thus, the dye removal percentage decreased in this acidic medium.

Figure 9 displays the influence of the adsorbent dose on the perecentage dye removal at an initial dye concentration (A) of 38.19 mg/L, pH (B) of nine, and time (D) of 89.75 min. The perecentage dye removal increased from 78.55 to 85.46% as the adsorbent dose increased from 200 to 1000 mg/L. This was because, as the adsorbent dose increased, the area of the surface expanded, generating a larger active sites number, thereby increasing a probability that the adsorbate could find active sites [9]. The slope being close to zero confirmed that the adsorbent dose had little influence on the responses.

Figure 10 illustrates the influence of the contact time on the perecentage dye removal at a constant initial dye concentration (A) of 38.19 mg/L, pH (B) of nine, and adsorbent dose (C) of 200 mg/L. The percentage dye removal increased from 68.44% to 78.6% as the time increased from 30 to 90 min. The results indicate the positive effect of the contact time on the perecentage dye removal.

3.4. Variables Combined Influence on the MB Dye Removal

This study investigated the influence of the initial dye concentration, pH of the solution, adsorbent dose, and contact time of the Fe_3O_4/CA on the MB dye removal as well as their joint influences.

Figure 11 illustrates the interaction between the initial dye concentration and pH at a constant contact time of 89.75 min and adsorbent dose of 200 mg/L. The MB removal from the aqueous solution increased as the pH of the solution increased from three to nine across the entire initial MB concentration range (up to 50 mg/L). This can be explained by the influence of the solution's pH on the adsorbent surface. Figure 12 shows the plot of pHf pHi versus pH. The positive values of the Fe_3O_4 changed to negative values = 7.6 (pH_{pzc}). At a pH of nine, the negatively charged surface of the adsorbent most significantly affected the adsorption of the MB dyes due to the electrostatic attraction between the negative surface charge and the cationic dye [39]. In contrast, at a pH of three, the protons competed with the MB dyes in trying to adsorb onto the available surfaces. As a result, the percentage removal decreased under these acidic conditions. These results confirmed those reported in earlier studies [40,41], which showed an increase in cationic dye adsorption with a rise in the pH level.
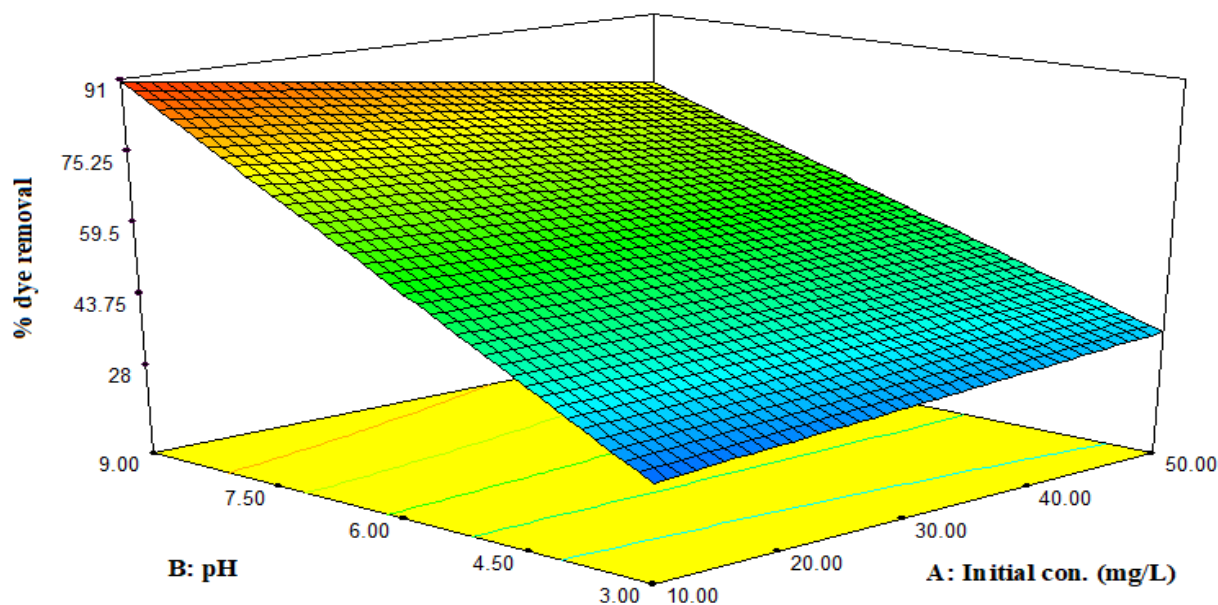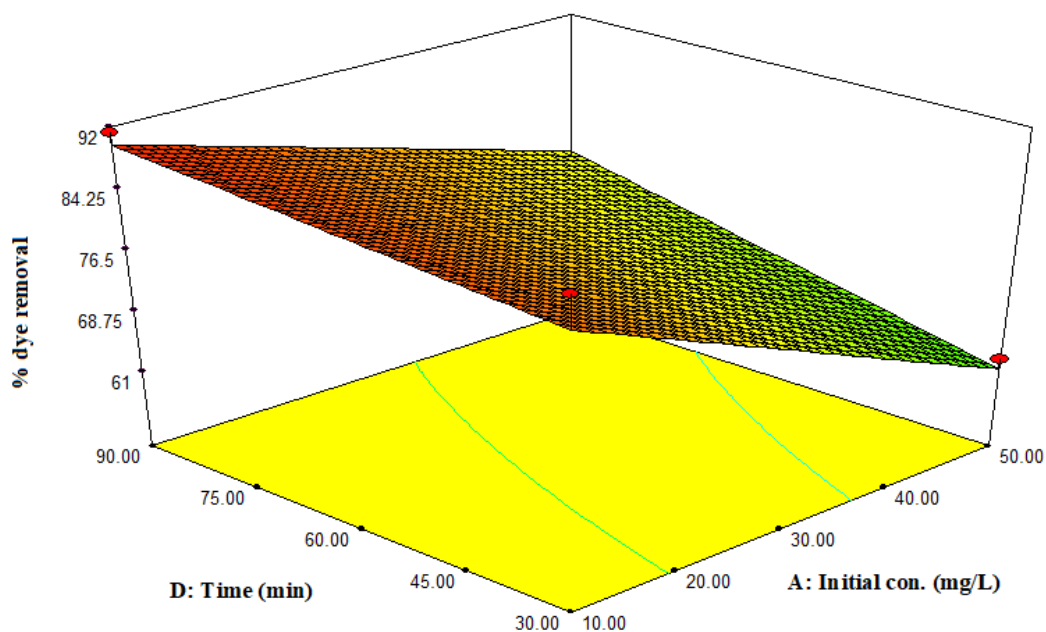
Figure 11. Interaction effect between the initial dye concontration (A) and the solution pH (B) on the perecentage dye removal at a constant contact time (D) of 89.75 min and adsorbent dose (C) of 200 (mg/L).
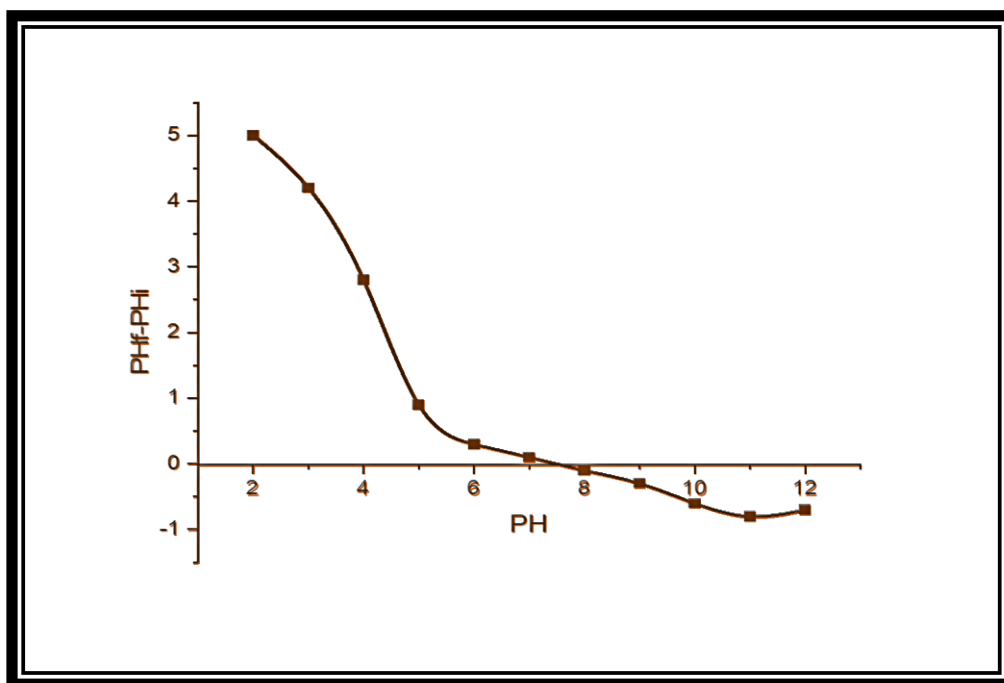

Figure 12. (pHf-pHi) versus pH for Fe_3O_4 NPs/CA.

Figure 13 shows the interactive effect of the initial dye concontration and contact time at a constant adsorbent dose and solution pH of Fe_3O_4/CA on the MB removal. It is obvious that the perecentage MB removal decreased as the MB concentration increased. This gives an indication that the active sites of adsorption were saturated on Fe_3O_4/CA surfaces. With the same MB initial concentration and various contact times, an increase in the contact time from 30 to 90 min caused an increase in the perecentage dye removal. Thus, it can be found that there were more active adsorbent sites on the Fe_3O_4/CA surfaces that were available and unoccupied to adsorb the dye molecules [42,43]. As can be seen in

Figure 14, the lines are not elliptical, which indicates that there is no interaction between the contact time and initial dye concentration.

Figure 13. Interaction effect between the contact time (D) and initial dye concentration (A) on the perecentage dye removal at a constant adsorbent dose (C) of 200 (mg/L) and a solution pH (B) of 9.
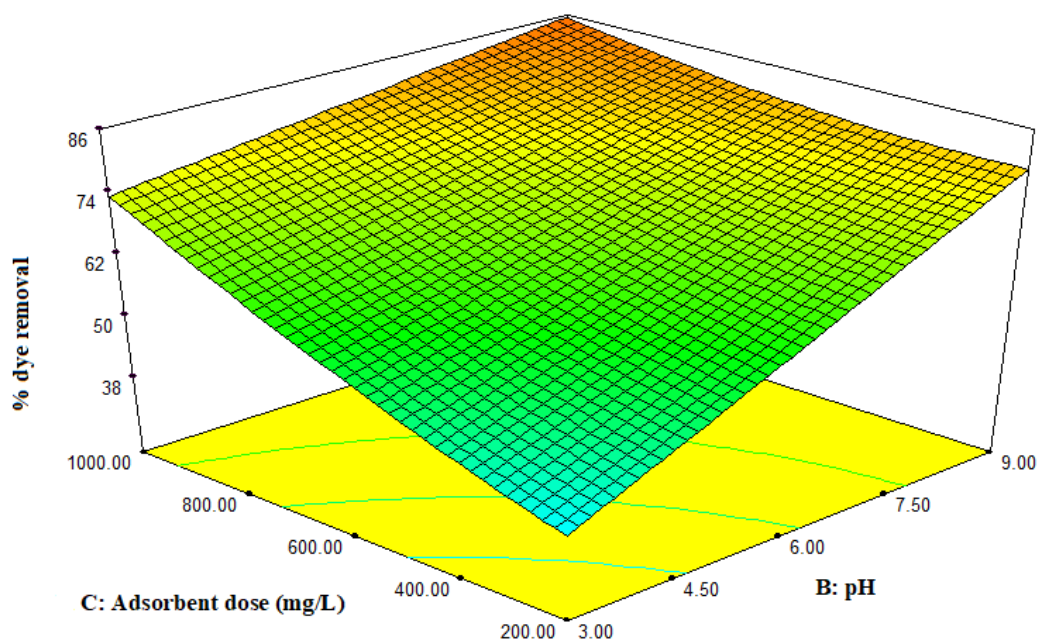
Figure 14. Interaction effect between the solution pH (B) and adsorbent dose (C) on the perecentage dye removal at a constant initial dye concontration (A) of 38.19 (mg/L) and contact time (D) of 89.75 min.

Figure 14 represents the effect of the solution's pH and adsorbent dosage at a fixed initial dye concontration of 38.19 mg/L and contact time of 89.75 min. It clearly shows that the adsorbent dosage had positive effects on the perecentage dye removal, whereas the removal efficiency increased with increases in the adsorbent dosage across the entire pH range (three–nine) of the solution. This may be attributed to the fact that the uptake was higher due to the availability of more active binding sites [44].

As can be seen in Figure 14, the lines are elliptical, which indicates that there is an interaction between the adsorbent dosage and pH of the solution.

The response surface plot for the effect of the pH and contact time on the removal efficiency at a constant initial dye concontration of 38.19 mg/L and adsorbent dose of 200 mg/L is shown in Figure 15. As the pH of the solution increased, the perecentage dye removal increased with the contact time from 30 to 90 min. This was due to the electrostatic interaction between the positively charged dye and the negatively charged adsorbent surface; the adsorption process worked best under these circumstances [45].
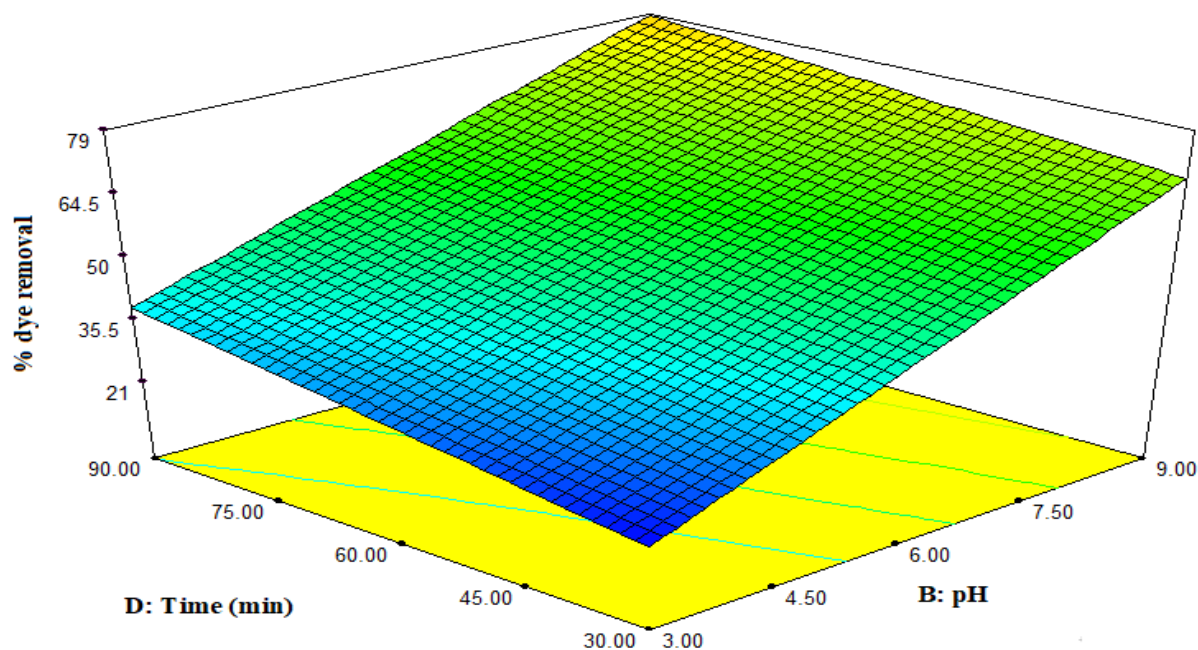

Figure 15. Interaction effect between the solution pH (B) and contact time (D) on the perecentage dye removal at a constant initial dye concontration (A) of 38.19 (mg/L) and adsorbent dose (C) of 200 (mg/L).

3.5. Optimization and Model Validation

Target criteria were set to maximize the perecentage MB removal to optimize the adsorption process, with four experimental parameters (i.e., initial dye concontration, solution pH, adsorbent dose, and contact time) chosen in the ranges considered in this study.

The optimal solution was based on a desirability value of one. Under optimal conditions, the best maximum perecentage dye removal of 93.14 was found to be at the initial dye concontration of 10.02 mg/L, the solution pH of 8.98, adsorbent dose of 997.99 mg/L, and contact time of 43.7 min (Figure 16). Additional experiments were conducted at the optimal experimental conditions in three replicates to validate the model's predicted results. The average MB removal efficiency of these three replicates was found to be 94%, which agrees with the predicted MB removal of 93.14%. This indicates the applicability of using a central composite design (CCD) to optimize and evaluate MB dye removal by Fe_3O_4/CA.
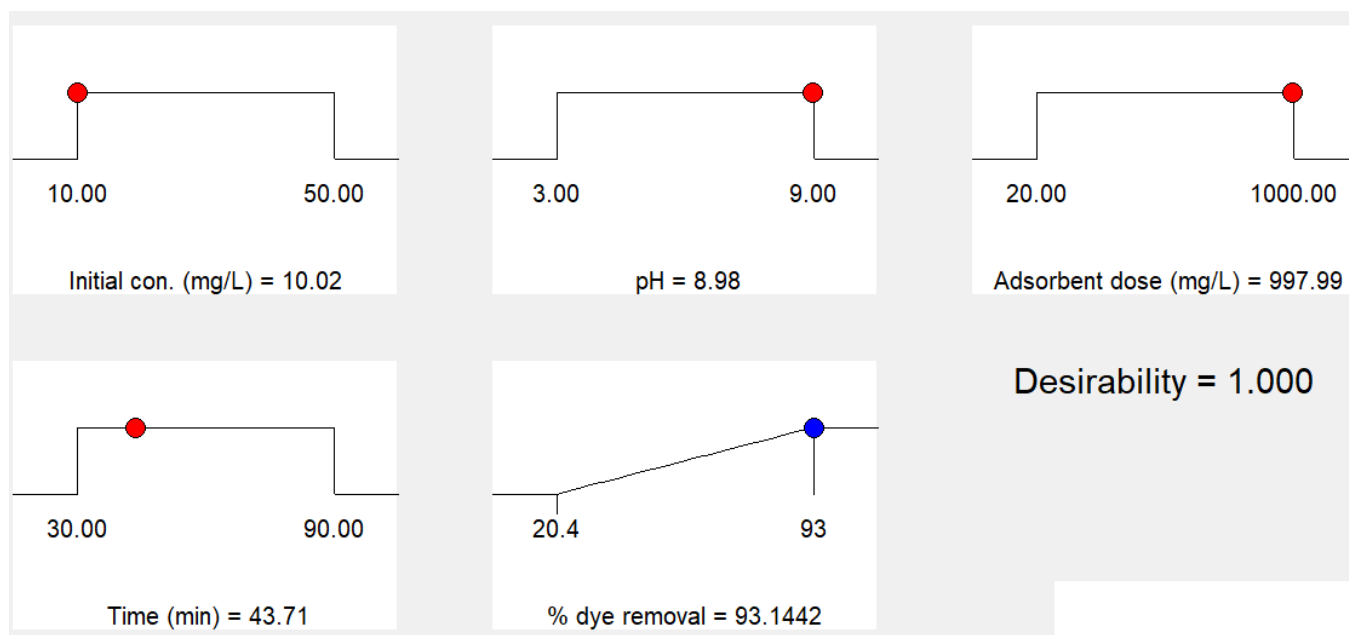
Figure 16. Ramp plot for the numerical optimized parameters.

3.6. Mechanism of Adsorption

The adsorption process is facilitated by various factors, including high surface area, high surface charge, and the presence of compatible functional groups. Of the total number of phenolic compounds, *C. aurantium* juice has been reported to contain 86% phenolic acids. A number of phenolic compounds are present in the *Citrus aurantium* juice (e.g., gallic, sinapic acid, dihydroxyphenilic acid, dihydrobenzoic acid, chlorogenic, vanillic, syringic, *p*-coumaric, ferulic, rosmarinic, trans-2-dihydrocinnamic, and cinnamic acids) [46]. According to the FTIR spectra of Fe_3O_4/CA, as shown in Figure 2b, a band at 1629 cm^{-1} and the broad band centered at 3435 cm^{-1} are related to the presence of hydroxyl groups and attributed to OH–bending and OH–stretching, respectively. The peaks between 1157.29 cm^{-1} and 1114.86 cm^{-1} are assigned to the stretching of between C–O and O–H for –COOH. Therefore, the phenolic and carboxylic groups played key roles in the adsorption mechanism.

In addition, the mechanisms of MB removal by the Fe_3O_4/CA adsorbent are illustrated in Figure 17. The bonding of hydrogen between the –OH groups of the Fe_3O_4/CA and an aromatic heterocyclic ring of the MB was a significant contributor in capturing the MB. Van der Waals forces between the phenolic ring of the adsorbent and aromatic heterocyclic ring of the MB may also have contributed.

The batch study data pointed that Fe_3O_4/CA exhibited better dye removal efficacy with a higher solution pH. This is possibly due to electrostatic interactions, because at a higher pH, the surface of the Fe_3O_4/CA tends to be negatively charged and interacts favorably with the positively charged MB dye. Thus, MB molecules were captured from water through Van der Waals forces, hydrogen bonding, and the electrostatic interaction.

3.7. Influence of Temperature

The influence of temperature on the MB dye removal was studied at 25, 30, and 35 °C, under the following conditions: The adsorbent dose of 998 mg/L, initial MB dye concentration of 10.02 mg/L, time of 43.7 min, and a solution pH of 8.98. The results indicated that the temperature had a small influence on the MB dye removal. For example, the dye removal efficiency increased from 93% to 95.49% by increasing the solution temperature from 293 to 308 K (Figure 18). This result demonstrated that the adsorption of MB on Fe_3O_4/CA was an endothermic process because, at higher temperatures, the dye molecules

diffused into the adsorbent. Reference [47] reported a similar observation, i.e., that the adsorption was an endothermic and spontaneous process.
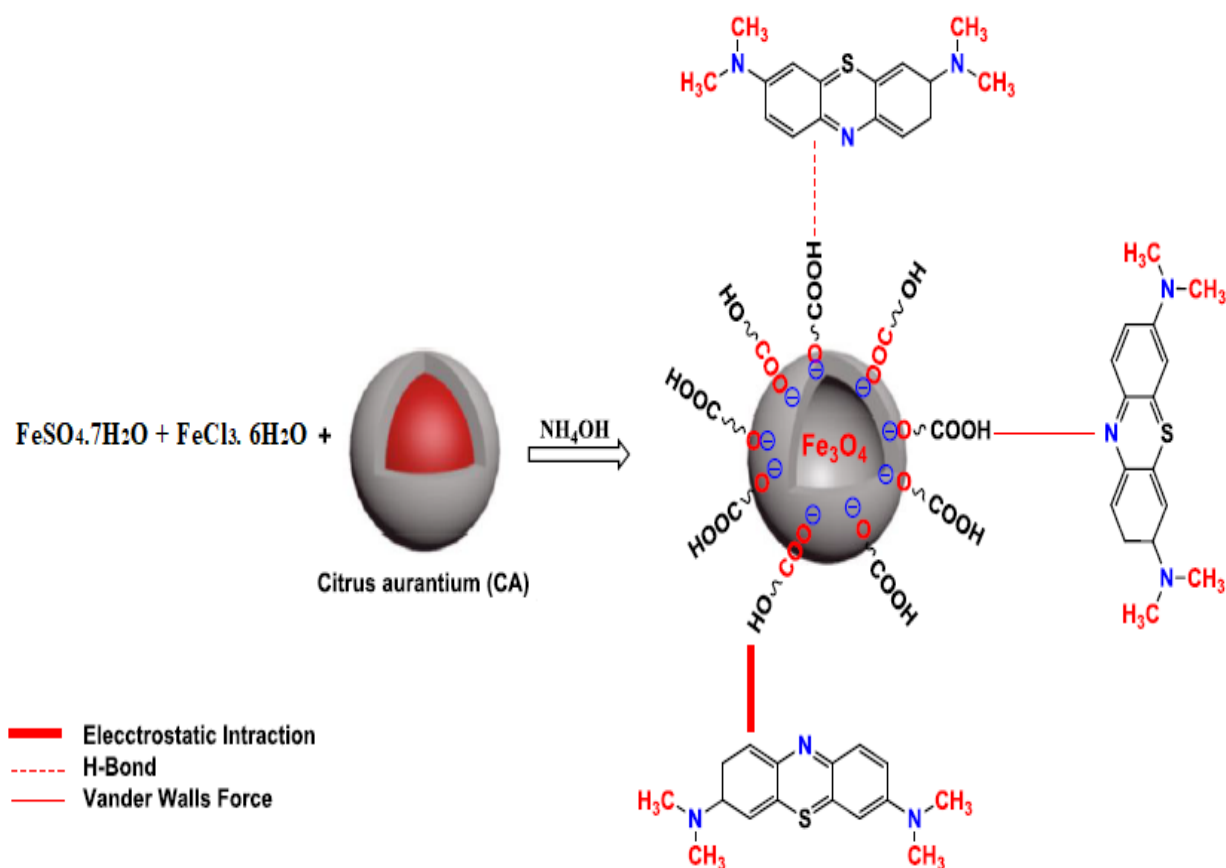

Figure 17. Proposed adsorption mechanisms of MB on Fe_3O_4.

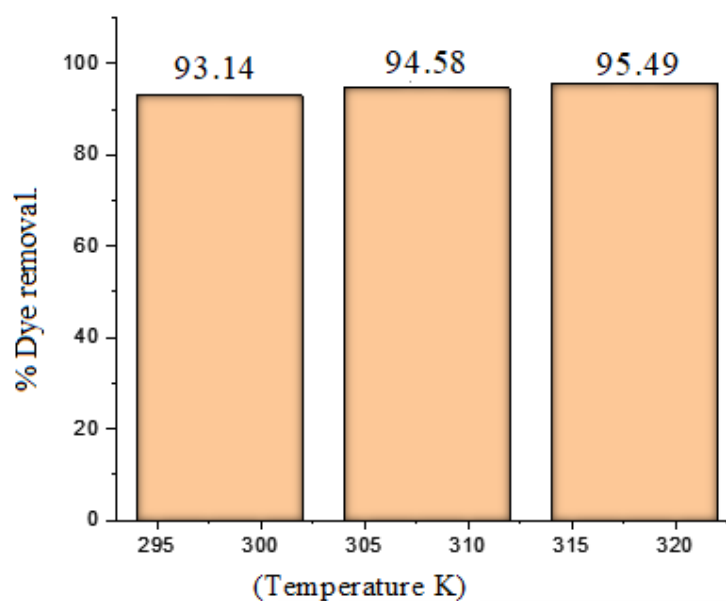**Figure 18.** Influence of the temperature on the perecentage dye removal.

3.8. Recycled Adsorption

Table 3 O_4/CA was studied in this work. Upon completion of the MB removal, the Fe_3O_4/CA particles were separated from the reaction mixture, washed with distilled water,

and reused for the removal of MB dye. As shown in Figure 19, the perecentage dye removal of Fe_3O_4/CA after five rounds of cyclic adsorption accounted for 93.14%, 92%, 91%, 88%, and 80.00% at the following conditions: pH = 8.98, adsorbent dose = 998 mg/L, initial concentration = 10.02 mg/L, and time = 43.7 min. Thus, the evidence indicates that Fe_3O_4NPs/CA is stable and reusable in removing MB dye from wastewater.
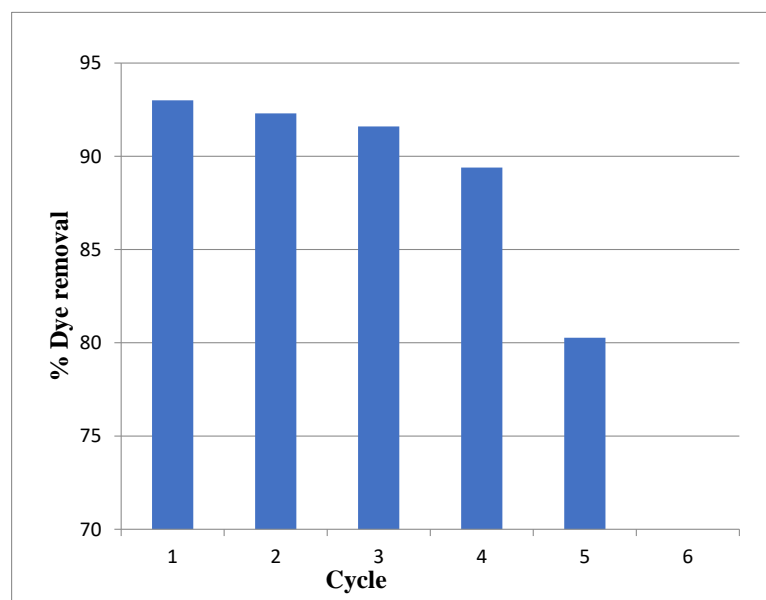
Figure 19. Cyclic adsorption performance of Fe_3O_4/CA.

3.9. Comparative Study of MB Dye Removal with Other Adsorbents

Table 6 shows the perecentage dye removal of MB by Fe_3O_4/CA compared to other adsorbents through the statistical experimental design at optimum conditions. It is evident that Fe_3O_4/CA is an efficient adsorbent for the removal of MB dye.

Table 6. Comparison of the perecentage dye removal of MB reported in extant studies with that of Fe_3O_4/CA.

Adsorbents	Optimum Conditions	% MB Dye Removal	Ref.
Activated carbon (AC) from grape leaves	pH (11), adsorbent dosage (12.5 g/L), MB initial concentration (100 mg/L), contact time (90 min)	97.4	[48]
Spruce sawdust (SD) coated by magnesium oxide (MgO)	pH (11), adsorbent dosage (3.50 g/L)	94.05	[49]
Cellulose dusts (CD)	pH (9.84), adsorbent dosage (4.38 g/L), MB concentration (75.50 mg/L), contact time (208.13 min)	98.05	[50]
Agricultural waste, cashew nut shell (CNS)	pH (10), adsorbent dose (2.1846 g/L), initial dye concentration (50 mg/L), contact time (62.8693 min)	100	[51]
Banana leaf ash (BLA)	Adsorbent dose (23.9 mg/100 mL), shaking time (3 h), shaking speed (356 rpm)	93.75	[52]
Zeolites 13X modified by magnetic nanoparticles	pH (8.93), adsorbent dose (1198 mg/L), temperature (53.39 °C), initial MB concentration (10.05 mg/L)	96	[12]
Fe_3O_4/CA	pH (8.98), adsorbent dose (997.99 mg/L), initial concentration of the dye (10.02 mg/L), contact time (43.7 min)	93.14	This work
Fe_3O_4		72.2	This work

4. Conclusions

In this paper, the extract of *Citrus aurantium* (CA) was employed in a green approach to prepare Fe_3O_4 nanoparticles. The green Fe_3O_4 NPs were used to reduce the amount of methylene blue dye in wastewater. In conclusion, these Fe_3O_4 NPs were successfully synthesized using an extract of *Citrus aurantium* (CA) via a green method. The results represented the Fe_3O_4/CA is an active adsorbent for MB removal from aqueous solutions, as 93.14% removal was conducted at an initial dye concentration of 10.02 mg/L, solution pH of 8.98, adsorbent dose of 997.99 mg/L, and contact time of 43.7 min. The solution pH (B) showed the essential effect on the perecentage dye removal, followed by adsorbent dose (C), interaction (BC), contact time (D), interaction (AB), and the initial dye concontration (A). The interactions terms (AD), (BD), and (C^2) had the lowest effects on the perecentage dye removal. The findings of this research support using green Fe_3O_4 NPs as an alternative and efficient adsorbent for MB dye removal in wastewater treatment.

Author Contributions: Conceptualization, S.B. and A.A.A.; methodology, S.B.; formal analysis, A.K.M.; investigation, A.K.M.; resources, H.S.M.; data curation, A.K.M.; writing—original draft preparation, S.B.; writing—review and editing, A.A.A.; visualization, A.K.M.; supervision, H.S.M.; administration of project, A.A.A. All authors have read and agreed to the published version of the manuscript.

Institutional Review Board Statement: Not applicable.

Informed Consent Statement: Not applicable.

Data Availability Statement: Not applicable.

Conflicts of Interest: We certify that they have no affiliations with or involvement in any organization or entity with any financial interest or nonfinancial interest in the subject matter or materials discussed in this manuscript.

References

1. Khalaf, I.H.; Al-Sudani, F.T.; AbdulRazak, A.A.; Aldahri, T.; Rohani, S. Optimization of Congo red dye adsorption from wastewater by a modified commercial zeolite catalyst using response surface modeling approach. *Water Sci. Technol.* **2021**, *83*, 369–1383. [CrossRef]
2. Mohammed, M.I.; Abdul Razak, A.A.; Hussein Al-Timimi, D.A. Modified multiwalled carbon nanotubes for treatment of some organic dyes in wastewater. *Adv. Mater. Sci. Eng.* **2014**, *2014*, 201052. [CrossRef]
3. Qasem NA, A.; Mohammed, R.H.; Lawal, D.U. Removal of heavy metal ions from wastewater: A comprehensive and critical review. *Npj Clean Water* **2021**, *4*, 36. [CrossRef]
4. Haounati, R.; Alakhras, F.; Ouachtak, H.; Saleh, T.A.; Al-Mazaideh, G.; Alhajri, E.; Jada, A.; Hafid, N.; Addi, A.A. Synthesized of Zeolite@Ag2O Nanocomposite as Superb Stability Photocatalysis Toward Hazardous Rhodamine B Dye from Water. *Arab J. Sci. Eng.* **2022**. [CrossRef]
5. Ouachtak, H.; El Guerdaoui, A.; Haounati, R.; Akhouairi, S.; El Haouti, R.; Hafid, N.; Addi, A.A.; Šljukić, B.; Santos DM, F.; Taha, M.L. Highly efficient and fast batch adsorption of orange G dye from polluted water using superb organo-montmorillonite: Experimental study and molecular dynamics investigation. *J. Mol. Liq.* **2021**, *335*, 116560. [CrossRef]
6. Ahmed, F.S.; Alsaffar, M.A.; AbdulRazak, A.A. One-step synthesis of magnetic fly ash composites for methylene blue removal: Batch and column study. *Environ. Sci. Pollut. Res.* **2022**. [CrossRef]
7. Garg, V.K. Green chemistry for dyes removal from waste water. *Green Process. Synth.* **2015**, *4*, 507–508. [CrossRef]
8. Abdulrazak, A.A.; Shakor, Z.M.; Rohani, S. Optimizing Biebrich Scarlet removal from water by magnetic zeolite 13X utilizing response surface method. *J. Environ. Chem. Eng.* **2018**, *6*, 6175–6183. [CrossRef]
9. Al-Dahri, T.; Abdulrazak, A.A.; Khalaf, I.H.; Rohani, S. Response surface modeling of the removal of methyl orange dye from its aqueous solution using two types of zeolite synthesized from coal fly ash. *Mater. Express* **2018**, *8*, 234–244. [CrossRef]
10. Al-Dahri, T.; Abdulrazak, A.A.; Rohani, S. Preparation and characterization of Linde-type A zeolite (LTA) from coal fly ash by microwave assisted synthesis method: Its application as adsorbent for removal of anionic dyes. *Int. J. Coal Prep. Util.* **2022**, *42*, 2064–2077. [CrossRef]

11. Abdulrazak, A.A.; Rohani, S. Sodium dodecyl sulfate modified Fe2O3/molecular sieves for removal of rhodamine B dyes. *Adv. Mater. Sci. Eng.* **2018**, *2018*, 3849867. [CrossRef]

12. Majid, Z.; Abdulrazak, A.A.; Noori, W.A.H. Modification of zeolite by magnetic nanoparticles for organic dye removal. *Arab J. Sci. Eng.* **2019**, *44*, 5457–5474. [CrossRef]

13. Ahmed, F.S.; Abdulrazak, A.A.; Alsaffar, M.A. Modelling and optimization of methylene blue adsorption from wastewater utilizing magnetic marble dust adsorbent: A response surface methodology approach. *Mater. Today Proc.* **2022**, *60*, 1676–1688. [CrossRef]

14. Babay, S.; Mhiri, T.; Toumi, M. Synthesis, structural and spectroscopic characterizations of maghemite γ—Fe_2O_3 pre pared by one—Step coprecipitation route. *J. Mol. Struct.* **2015**, *1085*, 286–293. [CrossRef]

15. Gubin, S.P.; Koksharov, Y.A.; Khomutov, G.B.; Yurkov, G.Y. Magnetic nanoparticles: Preparation, structure and properties. *Russ. Chem. Rev.* **2005**, *74*, 489–520. [CrossRef]

16. Belachew, N.; Rama Devi, D.; Basavaiah, K. Facile green synthesis of L-Methionine capped magnetite nanoparticles for adsorption of pollutant Rhodamine B. *J. Mol. Liq.* **2016**, *224*, 713–720. [CrossRef]

17. Kharissova, O.V.; Dias HV, R.; Kharisov, B.I.; Pérez, B.O.; Pérez, V.M.J. The greener synthesis of nanoparticles. *Trends Biotechnol.* **2013**, *31*, 240–248. [CrossRef]

18. Shejawal, K.P.; Randive, D.S.; Bhinge, S.D.; Bhutkar, M.A.; Wadkar, G.H.; Jadhav, N.R. Green synthesis of silver and iron nanoparticles of isolated proanthocyanidin: Its characterization, antioxidant, antimicrobial, and cytotoxic activities against COLO320DM and HT29. *J. Genet. Eng. Biotechnol.* **2020**, *18*, 43. [CrossRef]

19. Horst, M.F.; Coral, D.F.; van Raap, M.B.F.; Alvarez, M.; Lassalle, V. Hybrid nanomaterials based on gum Arabic and magnetite for hyperthermia treatments. *Mater. Sci. Eng. C* **2007**, *74*, 443. [CrossRef]

20. Madhuvilakku, R.; Alagar, S.; Mariappan, R.; Piraman, S. Green one-pot synthesis of flowers-like Fe_3O_4/rGO hybrid nanocomposites for effective electrochemical detection of riboflavin and low-cost supercapacitor applications. *Sens. Actuat. B Chem.* **2017**, *253*, 879–892. [CrossRef]

21. Win, T.T.; Khan, S.; Bo, B.; Zada, S.; Fu, P. Green synthesis and characterization of Fe_3O_4 nanoparticles using Chlorella-K01 extract for potential enhancement of plant growth stimulating and antifungal activity. *Sci. Rep.* **2021**, *11*, 21996. [CrossRef]

22. Ramesh, A.V.; Devi, D.R.; Botsa, S.M.; Basavaiah, K. Facile green synthesis of Fe_3O_4 nanoparticles using aqueous leaf extract of *Zanthoxylum armatum* DC. for efficient adsorption of methylene blue. *J. Asian Ceram.* **2018**, *6*, 145–155. [CrossRef]

23. Pepe, G.; Pagano, F.; Adesso, S.; Sommella, E.; Ostacolo, C.; Manfra, M.; Chieppa, M.; Sala, M.; Russo, M.; Marzocco, S.; et al. Bioavailable Citrus sinensis Extract: Polyphenolic Composition and Biological Activity. *Molecules* **2017**, *22*, 623. [CrossRef]

24. Khan, U.M.; Sameen, A.; Aadil, R.M.; Shahid, M.; Sezen, S.; Zarrabi, A.; Ozdemir, B.; Sevindik, M.; Kaplan, D.N.; Selamoglu, Z.; et al. Citrus Genus and Its Waste Utilization: A Review on Health-Promoting Activities and Industrial Application. *Evid. Based Complement. Alternat. Med.* **2021**, *2021*, 2488804. [CrossRef]

25. Karadeniz, F. Main organic acid distribution of authentic citrus juices in Turkey. *Turk. J. Agric. For.* **2004**, *28*, 267–271.

26. Massart, R. Preparation of Aqueous Magnetic Liquids in Alkaline and Acidic Media. *IEEE Trans. Magn.* **1981**, *17*, 1247–1248. [CrossRef]

27. Waldron, R.D. Infrared Spectra of Ferrites. *Phys. Rev.* **1955**, *99*, 1727–1735. [CrossRef]

28. Patrikiadou, E.; Patrikidou, A.; Hatzidaki, E.; Papandreou, C.N.; Zaspalis, V.; Nalbandian, L. Magnetic nanoparticles in Medical Diagnostic applications. Synthesis, characterization. functionalization and proteins conjugation. *Curr. Nanosci.* **2016**, *12*, 455–468.

29. Yan, P.; He, M.; Chen, B.; Hu, B. Restricted accessed nanoparticles for direct magnetic solid phase extraction of trace metal ions from human fluids followed by inductively coupled plasma mass spectrometry detection. *Analyst* **2015**, *140*, 4298–4306. [CrossRef]

30. Dovbeshko, G.I.; Gridina, N.Y.; Kruglova, E.B.; Pashchuk, O.P. FTIR spectroscopy studies of nucleic acid damage. *Talanta* **2000**, *53*, 233–246. [CrossRef]

31. Ragab, S.; El Nemr, A. Zirconyl chloride as a novel and efficient green Lewis acid catalyst for direct acetylation of cotton cellulose in the presence and absence of solvent. *J. Polym. Res.* **2019**, *26*, 156. [CrossRef]

32. He, H.; Gao, C. Supraparamagnetic, conductive, and processable multifunctional graphene nanosheets coated with high-density Fe_3O_4 nanoparticle. *ACS Appl. Mater. Interfaces* **2010**, *2*, 3201–3210. [CrossRef]

33. Smilgies, D.M. Scherrer grain-size analysis adapted to grazing-incidence scattering with area detectors. *J. Appl. Cryst.* **2009**, *42*, 1030–1034. [CrossRef]

34. Mascolo, M.C.; Pei, Y.; Ring, T.A. Room Temperature Co-Precipitation Synthesis of Magnetite Nanoparticles in a Large pH Window with Different Bases. *Materials* **2013**, *6*, 5549–5567. [CrossRef]

35. Altman, I.S.; Agranovski, I.E.; Choi, M. Mechanism of Nanoparticle Agglomeration during the Combustion Synthesis. *Appl. Phys. Lett.* **2005**, *87*, 053104. [CrossRef]

36. Chen, F.; Xie, S.; Zhang, J.; Liu, R. Synthesis of Spherical Fe_3O_4 Magnetic Nanoparticles by Co-Precipitation in Choline Chloride/Urea Deep Eutectic Solvent. *Mater. Lett.* **2013**, *112*, 177–179. [CrossRef]

37. Moosav, S.; Lai, C.W.; Gan, S.; Zamiri, G.; Pivehzhani, O.A.; Johan, M.R. Application of Efficient Magnetic Particles and Activated Carbon for Dye Removal from Wastewater. *ACS Omega* **2020**, *5*, 20684–20697. [CrossRef]

38. Shakor, Z.M.; Abdulrazak, A.A.; Shuhaib, A.A. Optimization of process variables for hydrogenation of cinnamaldehyde to cinnamyl alcohol over a Pt/SiO2 catalyst using response surface methodology. *Chem. Eng. Commun.* **2022**, *209*, 827–843. [CrossRef]
39. Borah, L.; Goswami, M.; Phukan, P. Adsorption of methylene blue and eosin yellow using porous carbon prepared from tea waste: Adsorption equilibrium, kinetics and thermodynamics study. *J. Environ. Chem. Eng.* **2015**, *3*, 1018–1028. [CrossRef]
40. Anirudhan, T.S.; Ramachandran, M. Adsorptive removal of basic dyes from aqueous solutions by surfactant modified bentonite clay (organoclay): Kinetic and competitive adsorption isotherm. *Process. Saf. Environ. Prot.* **2015**, *95*, 215–225. [CrossRef]
41. Hamdy, A.; Mostafa, M.K.; Nasr, M. Zero-valent iron nanoparticles for methylene blue removal from aqueous solutions and textile wastewater treatment, with cost estimation. *Water Sci. Technol.* **2018**, *78*, 367–378. [CrossRef]
42. Alsaiari, N.S.; Amari, A.; Katubi, K.M.; Alzahrani, F.M.; Rebah, F.B.; Tahoon, M.A. Innovative Magnetite Based Polymeric Nanocomposite for Simultaneous Removal of Methyl Orange and Hexavalent Chromium from Water. *Process* **2021**, *9*, 576. [CrossRef]
43. Yang, Y.; Yang, J.; Du, Y.; Li, C.; Wei, K.; Lu, J.; Chen, W.; Yang, L. Preparation and Characterization of Cationic Water—Soluble Pillar [5] arene Modified Zeolite for Adsorption of Methyl Orange. *ACS Omega* **2019**, *4*, 17741–17751. [CrossRef]
44. Zhang, J.; Zhou, Q.; Ou, L. Kinetic, isotherm, and thermodynamic studies of the adsorption of methyl orange from aqueous solution by chitosan/alumina composite. *J. Chem. Eng. Data* **2012**, *57*, 412–419. [CrossRef]
45. Igwegbe, C.A.; Mohmmadi, L.; Ahmadi, S.; Rahdar, A.; Khadkhodaiy, D.; Dehghani, R.; Rahdar, S. Modeling of adsorption of Methylene Blue dye on Ho-CaWO$_4$ nanoparticles using Response Surface Methodology (RSM) and Artificial Neural Network (ANN) techniques. *MethodsX* **2019**, *6*, 1779–1797. [CrossRef]
46. Tounsi, M.S.; Wannes, W.A.; Ouerghemmi, I.; Jegham, S.; Njima, Y.B.; Hamdaoui, G.; Zemni, H.; Marzouk, B. Juice components and antioxidant capacity of four Tunisian Citrus varieties. *J. Sci. Food. Agric.* **2011**, *91*, 142–151. [CrossRef]
47. Alguacil, F.J.; López, F. A Organic Dyes versus Adsorption Processing. *Molecules* **2021**, *26*, 5440. [CrossRef]
48. Mousavi, S.A.; Mahmoudi, A.; Amiri, S. Methylene blue removal using grape leaves waste: Optimization and modeling. *Appl. Water Sci.* **2022**, *12*, 112. [CrossRef]
49. Sharii, S.H.; Shoja, H. Optimization of process variables by response surface methodology for methylene blue dye removal using Spruce sawdust/MgO nano-biocomposite. *J. Water. Environ. Nanotechnol.* **2018**, *3*, 157–172.
50. Pajaie SH, S.; Archin, S.; Asadpou, G. Optimization of Process Parameters by Response Surface Methodology for Methylene Blue Removal Using Cellulose Dusts. *Civ. Eng. J.* **2018**, *4*, 620. [CrossRef]
51. Subramaniam, R.; Ponnusamy, S.K. Novel adsorbent from agricultural waste (cashew NUT shell) for methylene blue dye removal: Optimization by response surface methodology. *Water Resour. Ind.* **2015**, *11*, 64–70. [CrossRef]
52. Alam, Z.; Bari, N.; Kawsari, S. Statistical optimization of Methylene Blue dye removal from a synthetic textile wastewater using indigenous adsorbents. *Environ. Sustain. Indic.* **2022**, *14*, 100176. [CrossRef]